



Contents lists available at ScienceDirect

Quaternary International

journal homepage: www.elsevier.com/locate/quaint

Yangtze runoff, precipitation, and the East Asian monsoon in a 2800 years climate control simulation

Richard Blender^{a,*}, Xiuhua Zhu^a, Dan Zhang^{a,b,c}, Klaus Fraedrich^a

^a Meteorologisches Institut, Klima Campus, Universität Hamburg, Germany

^b Institute of Geographic Sciences and Natural Resources Research, Chinese Academy of Sciences, Beijing, China

^c Graduate School of the Chinese Academy of Sciences, Beijing, China

ARTICLE INFO

Article history:

Available online xxx

ABSTRACT

Variability of the Yangtze catchment hydrology is closely linked with the Tibetan Plateau snow cover and the large scale atmospheric circulation in East Asia. These connections are analyzed in a control simulation (2800 years) of the atmosphere–ocean general circulation model (ECHAM5/MPIOM) coupled to vegetation and ocean biogeochemistry modules. (i) Up to decades in time scale, runoff, soil wetness, and temperature show long term memory (LTM) with an intradecadal scaling of the power spectrum with the exponent $\beta \approx 0.6$, while precipitation, snow depth, and snow melt reveal no memory. (ii) Multi-decadal variability of runoff, soil wetness, and temperature shows weak LTM similar to snow depth and melt on the Tibetan Plateau. (iii) On the annual time scale, the atmospheric circulation impact of Hadley cell and ENSO on precipitation, temperature and snow melt are weak but significant; on decadal time scales the subtropical monsoon modulates the catchment hydrology. Temperature is anticorrelated with precipitation and soil wetness in the Yangtze catchment. Singular spectrum analysis highlights the 3–4 year ENSO mode in the monsoon indices, precipitation, and snow depth, explaining their high correlations. Projecting snow depth on ENSO shows long term variations explaining conflicting results obtained from correlations in short data sets.

© 2010 Elsevier Ltd and INQUA. All rights reserved.

1. Introduction

Interannual climate variability in East Asia affects the Yangtze River and its densely populated low terrain catchment, leading to disasters including floods or long-lasting wetness and drought conditions stressing natural vegetation and agriculture. Driving forces of the hydrological variability are the thermal contrasts between the high altitude snow on the Tibetan Plateau (TP) and the sea surface temperatures of the adjacent oceans which modulate the atmospheric circulation and the water cycle's storage and supply. Temperature and snow cover on the TP and the thermal inertia of the oceans are also the origin of (i) long term memory and (ii) interannual variability both of which lead to extreme events on different time scales. (iii) Finally, these forcings are embedded in the large scale circulation patterns and their dynamics.

Long term memory (LTM) is characterized by a non-exponential decay of the auto-correlation function; it extends to multi-decadal time scales and is detected by a power law decay of the power spectrum, $S(f) \sim f^{-\beta}$, with a positive exponent $\beta > 0$. LTM is

observed in many components of the hydrological cycle in East Asia (Blender and Fraedrich, 2006), such as soil temperature and wetness, and river discharges; precipitation, however, does not show memory on interannual time scales. LTM has also been detected in historical records of the last millennium indicating flood and droughts events in the Yangtze Delta (Jiang et al., 1997, 2005; Fraedrich and Zhu, 2009).

Precipitation in eastern China reveals variability on decadal and centennial time scales, appearing as trends in shorter data, which are not uniform and even with opposite signs in smaller regions (Becker et al., 2006; Qian et al., 2003a; Zheng et al., 2006). Periodicities are also reported (for summer precipitation) with periods of 15–35, 40–60, and 65–170 years, with long term variability of the corresponding amplitudes (Shen et al., 2009); Qian et al. (2003a) found a migrating dry/wet pattern with a period of 70 years. Standardized precipitation indices (SPI) obtained in instrumental data serve as indicators for wetness and drought conditions on different time scales and reveal variability up to decades (Bordi et al., 2004). No distinct relationship between precipitation and temperature in the Yangtze catchment (YC) has been identified (Zhang et al., 2008; Peng et al., 2009). Summer precipitation in the middle and the lower reaches of the YC is positively correlated with

* Corresponding author. Fax: +49 (0) 40 42838 5066.

E-mail address: Richard.Blender@zmaw.de (R. Blender).

the snow cover on the TP (Qian et al., 2003b; Wu and Qian, 2003). The fluctuations of TP glaciers are controlled by temperature, mainly during summer (Liang et al., 2008).

One of the large scale circulation patterns affecting the YC is the South Asian summer monsoon whose variability on decadal to centennial time scales (Duan et al., 2004) determines the YC precipitation. The established positive correlation of near surface land temperature and monsoon strength may change sign in global warming simulations (Sun et al., 2010); it is unknown whether such changes have occurred in the past. The East Asian summer monsoon is weaker during ENSO (El Niño/Southern Oscillation) warm phases (Kawamura, 1998; Ju and Slingo, 1995). However, this relationship varies on longer time scales due anomalies in the western North Pacific (Wu and Wang, 2002). Gershunov et al. (2001) have demonstrated that the relationship between ENSO and average Indian rainfall varies less for decadal means than for annual data and have interpreted these time scale dependent relationships as a stochastic effect.

A major restriction for a detailed analysis of long term climate variability is the short duration (about 50 years) of instrumental data in East Asia. However, there is a wealth of documentary records and proxy data for the most relevant hydrological impacts including floods and droughts in south-eastern China and the TP (Wang et al., 1991; Jiang et al., 2005; Qian et al., 2008; Holmes et al., 2009). However, in order to physically interpret these data for climatological reconstruction, their dynamic consistency and their highly significant interrelation with large scale circulation patterns are necessary prerequisites.

The aim of this paper is to determine the impact of internal climate variability on the interannual variability of the Yangtze runoff and the hydrological cycle in the catchment. To achieve this, a long term simulation (2800 years) was analyzed with a coupled atmosphere–ocean climate model (resolution $3.5^\circ \times 3.5^\circ$). The analysis includes monsoon indices, ENSO, and the snow cover on the TP. Correlation analysis yields highly significant correlations for annual and decadal means. Using singular spectrum analysis (SSA) the impact of the ENSO cycle is retrieved. To determine properties independent of specific external forcing conditions the analysis focuses on the internal variability in a constant climate without transient external forcings. As this study focuses on the long term memory (equivalent to enhanced low frequency variability), it is based on annual data. The correlations reveal dynamically consistent and significant relationships which might be practically useful for interpretation and reconstruction attempts using proxy and documentary data.

The paper is organized as follows: In Section 2 the model simulation, the analyzed data, and the applied methods are described. Results for short and long term memory are presented in Section 3 and correlations on different time scales including a singular spectrum analysis are derived in Section 4. Section 5 concludes with a Summary and a Discussion.

2. Simulated data and methods

The present analysis is based on the millennium experiments using the COSMOS-Atmosphere–Surface (Land)–Ocean-Biogeochemistry (ASOB) Earth System Model ('millennium run', Jungclauss et al., 2010). The model includes the atmospheric model ECHAM5 (Roeckner et al., 2003), the ocean model MPIOM (Marsland et al., 2003) and modules for land vegetation (JSBACH, Raddatz et al., 2007) and ocean biogeochemistry (HAMOCC, Wetzel et al., 2006), which are coupled via the OASIS3 coupler. The model includes the interactive simulation of the carbon cycle. ECHAM5 is run at T31 resolution ($\approx 3.75^\circ \times 3.75^\circ$) with 19 vertical levels, and MPIOM at a horizontal grid spacing of about 3° with 40 unevenly spaced

vertical levels. The present analysis focuses on the interannual variability and correlations during 2800 years of a control run (3000 years) for 800 AD with prescribed anthropogenic land-use (Foley et al., 2003; Pongratz et al., 2008).

2.1. Data

The analysis uses the following data sets (Fig. 1):

- (i) The Yangtze catchment (YC) with an area of $1.8 \cdot 10^6 \text{ km}^2$ is approximated by the model area extending from 100°E to 120°E and 25° to 35°N . The hydrology is based on annual mean catchment averages of precipitation (PRCP), near surface air temperature (2 m, TEMP), and soil wetness (WET). The Yangtze runoff (RUN) in the model is determined in the estuary (near 120°E , 31°N).
- (ii) The Tibetan Plateau (TP) is approximated by the area extending from 80°E to 92°E and 30°N to 37°N . Snow depth (SNOW) was analyzed to capture climatology and storage and snow melt (MELT) as the freshwater discharge.
- (iii) The Asian summer monsoon is characterized by two indices: MHI is the Monsoon Hadley circulation index (Goswami et al., 1999) defined as $\text{MHI} = V_{850} - V_{200}$, where the meridional velocities V are determined at 850 and 200 hPa in 70°E to 110°E and 10°N to 30°N . The MHI describes the South Asian (Indian) summer monsoon as part of the Hadley cell. EAMI is the East Asian Summer Monsoon Index, which describes the subtropical circulation and is defined by the difference in sea level pressure in 160°E to 110°E in 10°N to 50°N (Guo et al., 2004; Wei and Zhang, 2010). The El Niño/Southern Oscillation (ENSO) is described by sea surface temperature anomalies in the Niño3 region in the eastern tropical Pacific (5°S – 5°N , 90°W – 150°W).

Comparing the simulated control climate for 800 AD to the present-day observed and NCEP/NCAR re-analysis data (Kalnay et al., 1996) shows the following results:

The average model river runoff (RUN) is $50,600 \text{ m}^3/\text{s}$ ($31,900 \text{ m}^3/\text{s}$), the catchment temperature (TEMP) is 12.1°C (10°C – 15°C) and precipitation (PRCP) is $1730 \text{ mm}/\text{y}$ (1500 – $2500 \text{ mm}/\text{y}$). Soil wetness (WET), measured in volume fractions, is 0.66 (0.3 – 0.4) and the mean of the simulated snow depth on the TP (SNOW) is 0.009 m (0.006 m). The comparison reveals that, although the model simulates a past climate, the mean values are within the range of present-day observations. The differences are not only due to the model forcings and boundary conditions but also due to parameterizations of precipitation and soil hydrology, the low model resolution and the representation of the complex orography of East Asia.

2.2. Methods

In the present study short term memory is determined by the e-folding time τ (Wang et al., 2010), assuming an exponential decay of the auto-correlation function, $C(t) = \exp(-t/\tau)$. Long term memory is determined by (i) power spectra and (ii) detrended fluctuation analysis (DFA). All time series are standardized in the calculations. The power spectra are averages of the spectra calculated in 10 non-overlapping segments. The DFA is an efficient method to determine LTM in stationary time series (Peng et al., 1994; Fraedrich and Blender, 2003). The major application of the DFA is the extraction of power laws while oscillations (or cycles) should be analyzed by a standard power spectrum or periodogram. The DFA yields the fluctuation function $F(t)$ on the time scale t . For a power law in the power spectrum, $F(t) \sim t^\alpha$, the exponents are related by $\beta = 2\alpha - 1$. To determine $F(t)$ the anomalies are integrated to the profile which is partitioned in segments of length t , where linear fits

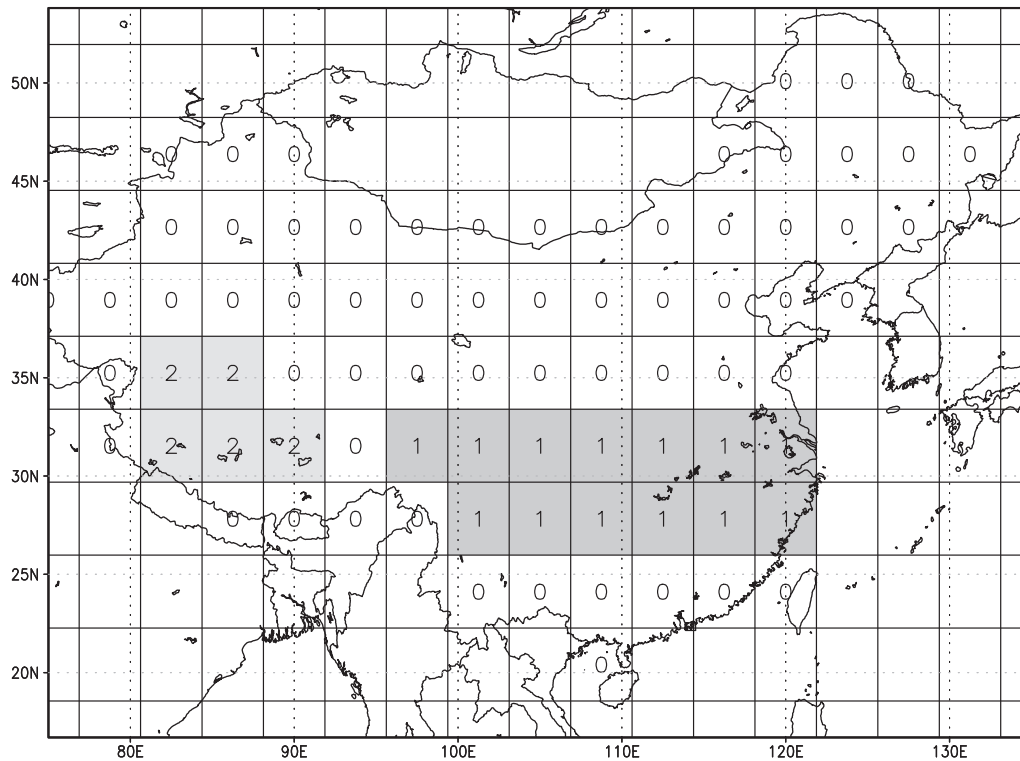


Fig. 1. Yangtze catchment (YC, "1") and Tibetan Plateau (TP, "2") in the grid cells of the model simulation ($\approx 3.75^\circ \times 3.75^\circ$).

are determined. The fluctuations $F(t)$ are the variances of the profile with respect to these fits averaged in all segments. The correlations are based on Pearson's correlation coefficient (Tables 1–3).

Singular spectrum analysis (SSA, Vautard and Ghil (1989), applied in a different context by Fraedrich (1986)) is used to determine modes of variability which cannot be associated with distinct spectral modes (for example the cyclic El Nino/Southern Oscillation). The SSA provides an adaptive spectral filter which decomposes variability according to dominant modes obtained in prescribed windows. In these windows, empirical orthogonal functions (EOFs, denoted as singular vectors) are determined which maximize the variability. The singular values describe the amount of variability in the corresponding vector. The principal components are obtained by projecting the data on the singular vectors, and the original time series can be retrieved (denoted as 'reconstruction') by sums of principal components multiplied by the singular vectors (this is analogous to the superposition of fields by EOFs). An oscillation in the data leads to a pair of singular vectors which are in quadrature (compare sine and cosine functions) and are used to reconstruct the periodic component of the data.

3. Short and long term variability

In this study, 'memory' is used equivalently to 'variability' to emphasize processes and time scales involved. Short term memory is characterized by the e-folding time τ . For the runoff and the soil wetness $\tau = 1$ year, while snow on the Tibetan Plateau (TP) decays distinctly faster, $\tau < 1$ year. The remaining data does not reveal a detectable e-folding time scale.

Long term memory (LTM) is present in a time series if the low frequency variability grows with decreasing frequency. In most practical circumstances the power spectrum follows a power law $S(f) \sim f^{-\beta}$ with $0 < \beta < 1$ for low frequencies. Absence of LTM is given for a white spectrum with $\beta = 0$. The limit $\beta = 1$ ($1/f$ spectrum or flicker noise) constrains stationarity. The exponential decay of the auto-correlation function changes to a power law decay, $C(t) \sim t^{-\gamma}$, with an exponent γ determined by $\gamma = 1 - \beta$. Long term memory is determined by power spectra and detrended fluctuation analysis (DFA), see Section 2.

The long term variability varies substantially in the compartments and reveals three main types.

Table 1

Correlations of annual hydrological time series within the Yangtze catchment and with Tibetan Plateau snow, monsoon indices and ENSO (only 99%-significant values are shown, $|r| > 0.1$).

Correlation coefficients (99%)		Yangtze catchment			Tibetan Plateau		Monsoon		ENSO
		PRCP	WET	TEMP	SNOW	MELT	MHI	EAMI	
Yangtze catchment	RUN	0.67	0.53	-0.28	0.12				
	PRCP		0.62	-0.14	0.13		-0.14	0.12	0.17
	WET			-0.33					
	TEMP								
Tibetan Plateau	SNOW				-0.15	-0.25	-0.31	-0.17	0.15
	MELT					0.73	-0.11	-0.10	0.26
							0.20	0.10	
Monsoon	MHI							0.63	-0.69
	EAMI								-0.61

Table 2
Correlations of decadal hydrological time series within the Yangtze catchment and with Tibetan Plateau snow, monsoon indices and ENSO (only 95%-significant values are shown, $|r|>0.1$).

Correlation coefficients (95%)		Yangtze catchment			Tibetan Plateau		Monsoon		ENSO
		PRCP	WET	TEMP	SNOW	MELT	MHI	EAMI	
Yangtze catchment	RUN	0.89	0.70	-0.31	0.11	0.17	0.11	0.16	
	PRCP		0.66	-0.12				0.13	
	WET			-0.39				0.15	
	TEMP						-0.15	-0.20	0.28
Tibetan Plateau	SNOW					0.69			
	MELT						0.29	0.10	-0.20
Monsoon	MHI							0.39	-0.66
	ESLP								-0.57

3.1. Yangtze catchment: scaling memory

Yangtze runoff and soil wetness in the catchment show a power spectrum with a power law for intradecadal frequencies (Fig. 2a), $S(f) \sim f^{-\beta}$, with $\beta \approx 0.6$. For low frequencies, the spectra of runoff, soil wetness, and temperature point to a weak memory on decadal time scales (Fig. 2b). The indicated power law exponent $\beta = 0.1$ is derived by DFA (see next paragraph). For precipitation the spectrum is white in the accessible frequency range (note that the white spectrum does not exclude long term variability).

The scaling of the power spectrum is substantiated by DFA (Fig. 3). In the intradecadal range the fluctuation functions for runoff and soil wetness increase approximately according to a power law $F(t) \sim t^\alpha$ with $\alpha = 0.8$. Using $\beta = 2\alpha - 1$, this corresponds to $\beta = 0.6$ marked in Fig. 2a. For longer time scales soil wetness, Yangtze runoff, and temperature show $\alpha = 0.55$, slightly deviating from a white spectrum memory ($\alpha = 1/2$); this is lower than $\alpha = 0.65-0.7$ obtained in observations and in a high resolution version of the atmospheric model ECHAM5 (Blender and Fraedrich, 2006).

Neglecting the low frequency scaling and assuming a (constant) white noise behavior, the power spectra of runoff, soil wetness, and temperature can be described by a modified red noise spectrum (Blender and Fraedrich, 2006).

$$S(f) = \frac{S_0}{1 + \left(\frac{f}{f_0}\right)^\beta} \quad (1)$$

where f_0 is the inverse time scale of the crossover between white noise for low frequencies and scaling memory for high frequencies. The standard red noise (Lorentzian) power spectrum is given for $\beta = 2$. This time scale is of the order of one decade for all variables in the YC (except for precipitation).

3.2. Tibetan Plateau: weak memory

Snow depth and snow melt on the Tibetan Plateau (TP) are considered to be main controls of the Yangtze discharge. The

variability of snow depth and snow melt reveal negligible inter-annual memory and a weak non significant spectral peak at the ENSO cycle of 3–4 years (Fig. 4a). Simulated snow cover on the TP reveals no long term memory. Therefore, according to this model simulation, the Yangtze discharge memory cannot be explained by the properties of snow on the TP. In the YC the long time scale of soil wetness appears to be the most likely process explaining the runoff variability. The absence of decadal periodicities detected by Qian et al. (2003a), for example, the 70 years Gleißberg cycle, confirms their external origin. The dominant types of variability are the quasi periodic ENSO and long term memory in the Yangtze catchment.

3.3. Monsoon and ENSO: periodicity

The monsoon indices EAMI, MHI, and ENSO show common characteristic spectra with a constant value for low frequencies and a distinct peak in the range of the ENSO cycle, 3–4 years (Fig. 4b). For higher frequencies the spectra decay rapidly with high exponents $\beta \gg 2$. The ENSO cycle dominates the variability of both monsoon indices. There is no oceanic long term memory involved in the tropical sea surface temperature, in contrast to, for example, the mid-latitude northern Atlantic ocean (Fraedrich and Blender, 2003).

4. Local and remote relationships

Hydrological processes in the Yangtze catchment (YC) are controlled by the large scale circulation and snow melt on the Tibetan Plateau (TP). To derive dynamically consistent long term relationships correlation coefficients for annual and decadal data are derived. The length of 2800 years enables the calculation of highly significant correlation coefficients for annual data as small as $|r| = 0.1$ with 99% significance (for decadal means with 95% significance). There are a large number of significant relationships within the YC and with snow on the TP, monsoon indices, and ENSO for annual data (Table 1, only values with 99% significance are included). For decadal means most of the relationships increase (Table 2, only values with 95% significance).

Table 3
Correlations of time series reconstructed by SSA for the first two singular vectors with the 3–4 years period ENSO mode (99% significance, $|r|>0.1$).

Correlation coefficients (99%)		Yangtze catchment			Tibetan Plateau		Monsoon		ENSO
		PRCP	WET	TEMP	SNOW	MELT	MHI	EAMI	
Catchment	PRCP				0.22		-0.27	-0.24	0.33
Tibetan Plateau	SNOW					0.72	-0.27	-0.33	0.51
	MELT						0.16		0.22
Monsoon	MHI							0.77	-0.73
	EAMI								-0.72

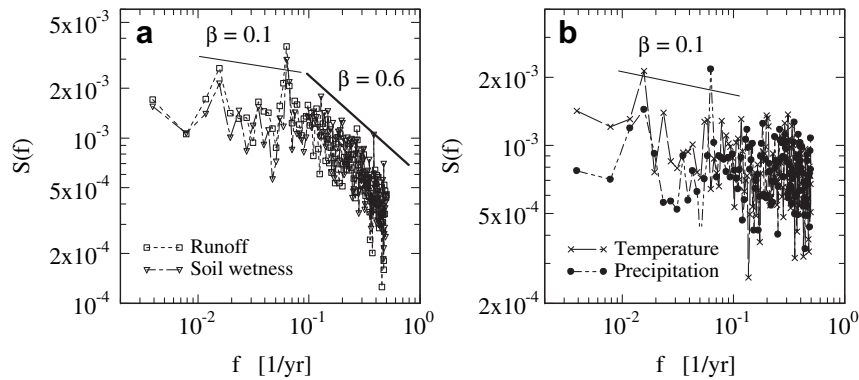


Fig. 2. Power spectra of (a) area averaged runoff and soil wetness, and (b) temperature and precipitation in the Yangtze catchment. The solid lines indicate power laws $S(f) \sim f^{-\beta}$ with exponents $\beta = 0.6$ (bold), and $\beta = 0.1$ (thin line).

4.1. Yangtze catchment

The relationships between runoff, precipitation and soil wetness in the catchment are distinct and obvious. There is a high anti-correlation between temperature and soil wetness, in particular on decadal time scales. The correlation between temperature and precipitation is negative but weak. In West China Holmes et al. (2009) report a positive correlation between temperature and precipitation. In a simulation for the last millennium, Peng et al. (2009) find no clear relationship between precipitation and temperature in East China.

4.2. Impacts of the Tibetan Plateau on the Yangtze catchment

Surprisingly, there is no (significant) correlation between annual Yangtze runoff and TP snow melt, and the correlation between runoff and snow depth is weak. A possible explanation is the weak variability of snow melt on time scales shorter than the ENSO cycle (Fig. 4a). For decadal means (Table 2) this changes significantly, probably due to the higher variability of snow melt on longer time scales.

The YC precipitation and TP snow depth are correlated on annual but not on decadal time scales. This agrees with the positive correlation between winter snow depth and subsequent summer rainfall in the catchment observed by Wu and Qian (2003) in station data during 1960–1998. According to the present analysis a possible underlying reason for the difference between annual and

decadal data is the common correlation with ENSO: TP snow depth and YC precipitation are correlated with ENSO on annual but not on decadal time scales.

4.3. Impacts of monsoon and ENSO

The monsoon indices MHI, EAMI, and ENSO are highly correlated on annual time scales (Table 1). Negative correlations between monsoon indices and ENSO are caused by cold anomalies in the western tropical Pacific reducing monsoon strength during ENSO warm events. On decadal time scales all correlations are weaker. A remarkable result is that the annual mean Yangtze runoff is neither correlated with southern and eastern Asian monsoon systems (MHI and EAMI) nor with ENSO; the decadal mean, however, shows the presumed monsoon control. Similarly, a significant relationship with the East Asian monsoon index EAMI exists for soil wetness only for decadal means.

Some further relationships are noted:

- (i) The Indian summer monsoon index MHI determines annual YC precipitation, temperature, and TP snow melt variability. For decadal averages the impact decreases in the YC and increases for TP snow melt.
- (ii) On decadal time scales the hydrology in the YC is controlled by the East Asian summer monsoon index EAMI. There is a strong impact of ENSO on temperature in the YC, accompanied by reduced TP snow melt.
- (iii) Negative correlations between near surface land temperature and monsoon strength are found in global warming simulations and are ascribed to the reduction of upper level thermal contrast (see the discussion in Sun et al. (2010)). However, this result depends crucially on the definition of the monsoon index, for example if the monsoon index is defined by the vertical shear (850–200 hPa) of the zonal wind in 100–130°E, 0–10°N, the correlation with temperature in the YC is positive, $r = 0.23$, and vanishes for decadal means.

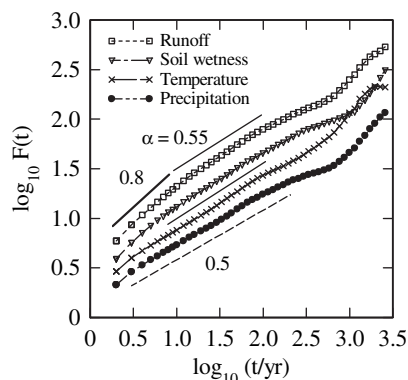


Fig. 3. DFA fluctuation functions of area averaged runoff, soil wetness, temperature, and precipitation in the Yangtze catchment. The solid lines indicate power laws in the fluctuation function $F(t) \sim t^\alpha$, $\alpha = 0.8$ (bold), $\alpha = 0.55$ (thin solid), and $\alpha = 0.5$ (dashed, no memory).

4.4. ENSO mode: singular spectrum analysis

The spectral and the correlation analyses reveal that ENSO dominates the variability of the hydrological cycle of the YC and the TP. To unveil the ENSO mode as the major origin for the correlations singular spectrum analysis is used as a data adaptive filter to extract the ENSO mode in the annual time series (see Section 2.2). The SSA is applied with a window of ten years and the time series with the 3–4 years ENSO mode as the first two singular vectors are selected

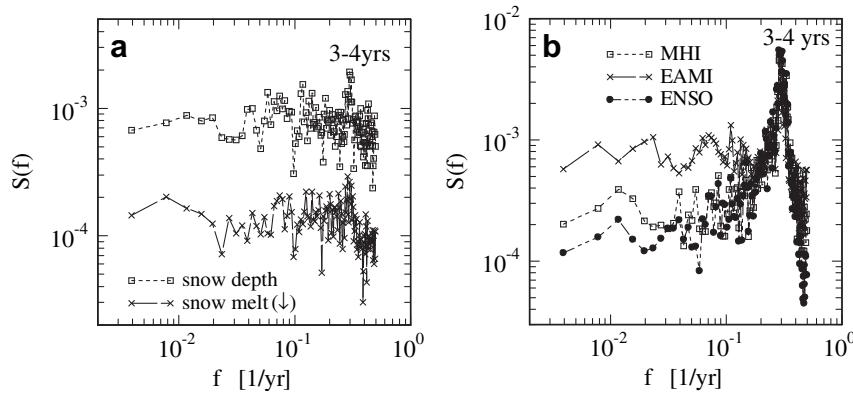


Fig. 4. Power spectra of (a) area averaged snow depth and snow melt (shifted) on the Tibetan Plateau and (b) monsoon indices and ENSO. All spectra in (b) are peaked at 3–4 years.

for further analysis; this includes precipitation in the YC, snow depth and snow melt on the TP, and both monsoon indices. For these time series the first two singular vectors and the principal components are used to reconstruct the data which is subject to a correlation analysis (Table 3) revealing distinctly higher values compared to annual and decadal means (Tables 1 and 2).

As an example the correlation of ENSO with the TP snow depth is studied in more detail. The first two singular values of the ENSO eigenvalue spectrum (Fig. 5a) represent the dominant oscillatory mode represented by the singular vectors in 3–4 years (Fig. 5b); both singular values contribute roughly 60% to the total variability. Snow depth shows a smooth spectrum of singular values, the first two vectors coincide with the ENSO mode (Fig. 5a and b). The structure of the two vectors in both time series supports the coherency of the two time series in the corresponding frequency band. The next two singular vectors (indices 3, 4) do not support a linear oscillation.

The reconstruction using the first two vectors and the associated principal components represent the oscillatory 3–4 years variability prescribed by the ENSO mode. An exemplary snapshot of the reconstructed time series with 200 years duration (Fig. 6) shows that ENSO and snow depth are in phase with varying amplitudes. While there are long term periods when both amplitudes are of similar magnitude (for example during the years 100–190), extended intervals when the snow amplitude is much weaker than the ENSO amplitude can also be found (see 190–300 years). The weak amplitude of snow depth in this SSA-reconstruction leads to a reduced correlation in the original data: in the first period (100–190 years) the correlation in the data is $r = 0.21$, and in the second period (190–300 years), $r = 0.16$. This result is in agreement with findings denoted as unstable or conflicting correlations

between ENSO and other indices (for example Ju and Slingo, 1995; Gershunov et al., 2001; Wu and Wang, 2002).

5. Summary and discussion

This study analyses the variability of the Yangtze runoff and the embedding in regional and remote teleconnections in a model environment without variable external forcing. The data is based on 2800 years of a control simulation for 800 AD climate conditions with a complex atmosphere–ocean general circulation model (ECHAM5/MPIOM) coupled to modules for land vegetation and ocean biogeochemistry. In the Yangtze catchment (YC) precipitation, soil wetness, and atmospheric near surface temperature, and on the Tibetan Plateau (TP) snow depth and melt are included. The large scale circulation indices considered are the East Asian summer monsoon (EAMI), the South Asian summer monsoon (MHI), and the El Niño/Southern Oscillation (ENSO).

A first part of the study determines short and long term variabilities. Runoff, soil wetness, and temperature show memory up to decades with a scaling behavior (exponent $\beta \approx 0.6$), while precipitation reveals no memory. For longer time scales runoff, soil wetness, and temperature show weak long term memory similar to snow depth and snow melt on the TP. The variability of the monsoon is controlled by the ENSO mode. The ENSO cycle is detectable in the TP snow depth and snow melt, but not in the Yangtze catchment hydrology.

A second part is given by significant and dynamically consistent relationships between the Yangtze runoff, the catchment hydrology, TP snow cover, Asian summer monsoon, and ENSO. Thanks to the long simulation period highly significant (99%) correlation coefficients for annual data, and significant (95%)

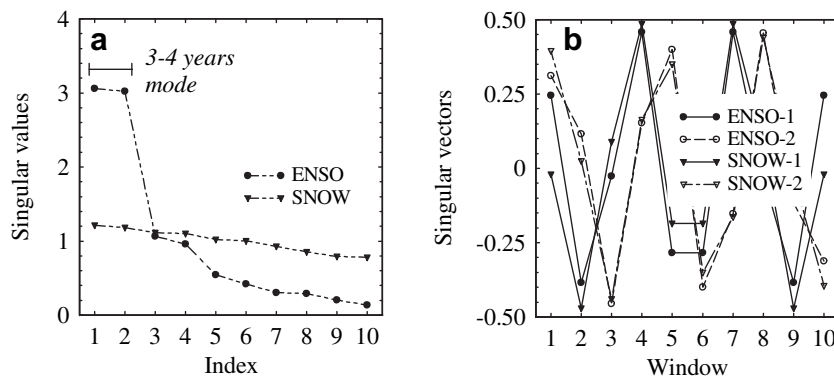


Fig. 5. (a) Singular values of the singular spectrum analysis (SSA) for ENSO and snow depth on the Tibetan Plateau; the first two are the 3–4 years ENSO mode. (b) The first two SSA singular vectors for both variables.

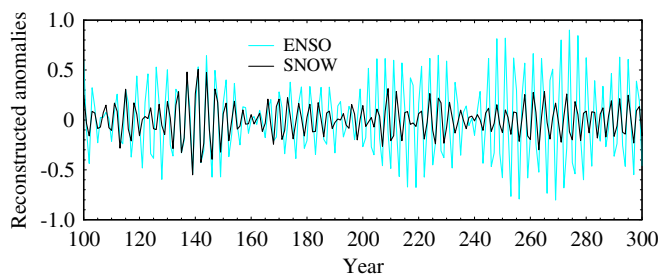


Fig. 6. Reconstructed time series for ENSO (grey) and snow depth SNOW (solid) using the first two SSA modes (ENSO mode) and the principal components (snapshot during the years 100–300).

indices are retrieved for decadal means with $|r| > 0.1$ threshold. On an annual basis there are significant correlations between YC temperature and MHI, and between TP snow depth and ENSO. Noteworthy are the high correlation coefficients between decadal means of TP snow melt and Indian summer monsoon (MHI), and between YC temperature and ENSO. For annual means the Indian summer monsoon dominates the YC climate while for decadal means the East Asian summer monsoon dominates, i.e. there is a shift from a tropical to a subtropical influence depending on the time scales. Temperature is anticorrelated with precipitation and soil wetness in the YC for annual and decadal means.

The ENSO mode with the 3–4 year cycle exerts a dominating influence on the East Asian climate. The Singular Spectrum Analysis (SSA) reveals that the monsoon indices, precipitation in the YC, and snow depth and melt on the TP show the ENSO mode in the first two singular vectors. The correlations between the reconstructed ENSO modes in these time series are distinctly higher than for the annual and decadal means of the original data. To study time-varying relationships the TP snow depth is analyzed as an example for one of the most relevant forcings for the YC. While the reconstructed snow depth and ENSO are in phase, the amplitudes show long term variations explaining conflicting results in short data sets. This long term variability could have its origin in compartments with long term memory such as soil wetness or the sea surface temperature in the adjacent oceans.

The relationships identified by the correlation analysis might have implications for climate reconstruction based on proxy and documentary data. The high significance allows extracting relationships which can be masked by trends and long term variability in shorter data sets. The dynamically consistent relationships enable validation of climate reconstructions based on statistical approaches applied to proxy data.

The study focuses on annual data to determine the long term variability and to provide a basis for the comparison with climate reconstructions, for which annual and long term mean data are available. For most of the variables considered, for example, the Yangtze runoff, the attribution of the annual values to the season with maximum contribution is feasible. For a further analysis of the processes in East Asia a higher resolution atmospheric model version is preferable with a more detailed representation of the complex orography.

Acknowledgements

We would like to thank Johann Jungclaus, Martin Claußen, and the Millennium consortium at the Max-Planck Institute and at the University of Hamburg for providing the simulated data and stimulating discussions. We are grateful for the suggestions of two anonymous reviewers. DZ acknowledges the support for the visit to

Klima Campus by the Institute of Geographic Sciences and Natural Resources Research (Chinese Academy of Sciences) and the Graduate School of the Chinese Academy of Sciences. XZ, KF, and RB acknowledge participation at the Conference on Large Asian Rivers in Wuhan, October 25–29, 2009 (Sino-German collaboration project ‘Climate Change Floods and Droughts’ (CCFD), the Mercator Foundation, and the Max-Planck Fellow group).

References

- Becker, S., Gemmer, M., Jiang, T., 2006. Spatiotemporal analysis of precipitation trends in the Yangtze River catchment. *Stochastic Environmental Research and Risk Assessment* 20, 435–444. doi:10.1007/s00477-006-0036-7.
- Blender, R., Fraedrich, K., 2006. Long term memory of the hydrological cycle and river runoffs in China in a high resolution climate model. *International Journal of Climatology* 26, 1547–1565.
- Bordi, I., Fraedrich, K., Jiang, J.M., Sutera, A., 2004. Spatio-temporal variability of dry and wet periods in eastern China. *Theoretical and Applied Climatology* 79, 81–91.
- Duan, K., Yao, T., Thompson, L.G., 2004. Low-frequency of southern Asian monsoon variability using a 295-year record from the Dasuopu ice core in the central Himalayas. *Geophysical Research Letters* 31 (L16209). doi:10.1029/2004GL020015.
- Foley, J.A., Delire, C., Ramankutty, N., Snyder, P., 2003. Green surprise? How terrestrial ecosystems could affect Earth's climate. *Frontiers of Ecology and Environment* 1, 38–44.
- Fraedrich, K., 1986. Estimating the dimensions of weather and climate attractors. *Journal of Atmospheric Science* 43, 419–432.
- Fraedrich, K., Blender, R., 2003. Scaling of atmosphere and ocean temperature correlations in observations and climate models. *Physical Review Letters* 90, 108501.
- Fraedrich, L., Zhu, X., 2009. Yangtze discharge memory. *Quaternary Sciences* 29, 696–700.
- Gershunov, A., Schneider, N., Barnett, T., 2001. Low-frequency modulation of the ENSO–Indian monsoon rainfall relationship: signal or noise? *Journal of Climate* 14, 2486–2492.
- Goswami, B.N., Krishnamurthy, B., Annamalai, H., 1999. A broad-scale circulation index or interannual variability of the Indian summer monsoon. *Quarterly Journal, Royal Meteorological Society* 125, 611–633.
- Guo, Q.Y., Cai, J.N., Shao, X.M., 2004. Studies on the variations of East-Asian summer monsoon during AD 1873–2000. *Chinese Journal of Atmospheric Sciences* 28, 206–216 (in Chinese).
- Holmes, J.A., Cook, E.R., Yang, B., 2009. Climate change over the past 2000 years in Western China. *Quaternary International* 194, 91–107.
- Jiang, J., Zhang, D., Fraedrich, K., 1997. Historic climate variability of wetness in east China (960–1992): a wavelet analysis. *International Journal of Climatology* 17, 969–981.
- Jiang, T., Zhang, Q., Blender, R., Fraedrich, K., 2005. Yangtze delta floods and droughts of the last millennium: abrupt changes and long term memory. *Theoretical and Applied Climatology* 82, 131–141.
- Ju, J., Slingo, J., 1995. The Asian summer monsoon and ENSO. *Quarterly Journal, Royal Meteorological Society* 121, 1133–1168.
- Jungclaus, J.H., Lorenz, S.J., Timmreck, C., Reick, C.H., Brovkin, V., Six, K., Segsneider, J., Giorgetta, M.A., Crowley, T.J., Pongratz, J., Krivova, N.A., Vieira, L.E., Solanki, S.K., Klocke, D., Botzet, M., Esch, M., Gayler, V., Haak, H., Raddatz, T.J., Roeckner, E., Schnur, R., Widmann, H., Claussen, M., Stevens, B., Marotzke, J., 2010. Climate and carbon-cycle variability over the last millennium. *Climate of the Past Discussions* 6, 1009–1044. doi:10.5194/cpd-6-1009-2010.
- Kalnay, E., Kanamitsu, M., Kistler, R., Collins, W., Deaven, D., Gandin, L., Iredell, M., Saha, S., White, G., Woollen, J., Zhu, Y., Chelliah, M., Ebisuzaki, W., Higgins, W., Janowiak, J., Mo, K.C., Ropelewski, C., Wang, J., Leetmaa, A., Reynolds, R., Jenne, R., Joseph, D., 1996. The NCEP/NCAR 40-year reanalysis project. *Bulletin of the American Meteorological Society* 77 (3), 437–471.
- Kawamura, R., 1998. A possible mechanism of the Asian summer monsoon-ENSO coupling. *Journal of the Meteorological Society of Japan* 76, 1009–1027.
- Liang, E., Shao, X., Qin, N., 2008. Tree-ring based summer temperature reconstruction for the source region of the Yangtze River on the Tibetan Plateau. *Global and Planetary Change* 61, 313–320.
- Marsland, S., Haak, H., Jungclaus, J., Latif, M., Röske, F., 2003. The Max-Planck-Institute global ocean/sea ice model with orthogonal curvilinear coordinates. *Ocean Modeling* 5, 91–127.
- Peng, C.K., Buldyrev, S.V., Havlin, S., Simons, M., Stanley, H.E., Goldberger, A.L., 1994. On the mosaic organization of DNA sequences. *Physical Review E* 49, 1685–1689.
- Peng, Y.B., Xu, Y., Jin, L., 2009. Climate changes over eastern China during the last millennium in simulations and reconstructions. *Quaternary International* 208, 11–18.
- Pongratz, J., Reick, C., Raddatz, T., Claussen, M., 2008. A reconstruction of global agricultural areas and land cover for the last millennium. *Global Biogeochemical Cycles* 22 (GB3018). doi:10.1029/2007GB003153.
- Qian, W., Hu, Q., Zhu, Y., Lee, D.-K., 2003a. Centennial-scale dry–wet variations in East Asia. *Climate Dynamics* 21, 77–89.

- Qian, Y.F., Zheng, Y.Q., Zhang, Y., Miao, M.Q., 2003b. Responses of China's summer monsoon climate to snow anomaly over the Tibetan Plateau. *International Journal of Climatology* 23, 593–613.
- Qian, W., Ding, T., Fu, J., Lin, X., Zhu, Y., 2008. Review on the data application and climate variability in China for various timescales. *Advances in Climate Change Research Supplement* 4, 1–6.
- Raddatz, T.J., Reick, C.J., Knorr, W., Kattge, J., Roeckner, E., Schnur, R., Schnitzler, K.G., Wetzol, P., Jungclaus, J.H., 2007. Will the tropical land biosphere dominate the climate-carbon cycle feedback during the 21st century? *Climate Dynamics* 29, 565–574.
- Roeckner, E., Bäuml, G., Bonaventura, L., Brokopf, R., Esch, M., Giorgetta, M., Hagemann, S., Kirchner, I., Kornblueh, L., Manzini, E., Rhodin, A., Schlese, U., Schulzweida, U., Tompkins, A., 2003. The Atmospheric General Circulation Model ECHAM5. Part I: Model Description. Max Planck Institute for Meteorology, Report, vol. 349 127pp.
- Shen, C., Wang, W.C., Peng, Y., Xu, Y., Zheng, J., 2009. Variability of summer precipitation over eastern China during the last millennium. *Climate of the Past* 5, 129–141.
- Sun, Y., Ding, Y., Dai, A., 2010. Changing links between South Asian summer monsoon circulation and tropospheric land–sea thermal contrasts under a warming scenario. *Geophysical Research Letters* 37 (L02704). doi:10.1029/2009GL041662.
- Vautard, R., Ghil, M., 1989. Singular spectrum analysis in nonlinear dynamics, with applications to paleoclimatic time series. *Physica D* 35, 395–424.
- Wang, R., Wang, S., Fraedrich, K., 1991. An approach to reconstruction of temperature on seasonal basis using historical documents from China. *International Journal of Climatology* 11, 381–392.
- Wang, G., Dolman, A.J., Blender, R., Fraedrich, K., 2010. Fluctuation regimes of soil moisture in ERA-40 re-reanalysis data. *Theoretical and Applied Climatology* 99, 1–8. doi:10.1007/s00704-009-0111-3.
- Wei, F.Y., Zhang, T., 2010. Oscillation characteristics of summer precipitation in the Huaihe River valley and relevant climate background. *Science China Earth Sciences* 53 (2), 301–316. doi:10.1007/s11430-009-0151-7.
- Wetzol, P., Maier-Reimer, E., Keenlyside, N., Botzet, M., Latif, M., Jungclaus, J.H., 2006. Effects of ocean biology on the penetrative radiation in a coupled climate model. *Journal of Climate* 19, 3973–3987.
- Wu, R., Wang, B., 2002. A contrast of the East Asian summer monsoon–ENSO relationship between 1962–1977 and 1978–1992. *Journal of Climate* 15, 3266–3279.
- Wu, T.-W., Qian, Z.-A., 2003. The relation between the Tibetan winter snow and the Asian summer monsoon and rainfall: an observational investigation. *Journal of Climate* 16, 2038–2051.
- Zhang, Q., Gemmer, M., Chen, J., 2008. Climate change and flood/drought risk in the Yangtze delta, China, during the past millennium. *Quaternary International* 176–177, 62–69.
- Zheng, J., Wang, W.-C., Ge, Q., Man, Z., Zhang, P., 2006. Precipitation variability and extreme events in Eastern China during the past 1500 years. *Terrestrial Atmospheric and Oceanic Sciences* 17 (3), 579–592.